Received: 26 November 2017 | Revised: 3 April 2018 | Accepted: 4 April 2018

DOI: 10.1002/chir.22969

SPECIAL ISSUE ARTICLE

WILEY

HPLC-ECD and TDDFT-ECD study of hexahydropyrrolo[1,2-a]quinoline derivatives

László Tóth[1,2] | Attila Mándi[1] | Dániel Váradi[1] | Tibor Kovács[1] | Anna Szabados[1] | Attila Kiss-Szikszai[1] | Qi Gong[3] | Haiyan Zhang[3] | Péter Mátyus[4] | Sándor Antus[1] | Tibor Kurtán[1]

[1]Department of Organic Chemistry, University of Debrecen, Debrecen, Hungary

[2]Department of Organic Chemistry, Semmelweis University, Budapest, Hungary

[3]CAS Key Laboratory of Receptor Research, Shanghai Institute of Materia Medica, Chinese Academy of Sciences, Shanghai, China

[4]Institute of Digital Health Sciences, Semmelweis University, Budapest, Hungary

Correspondence
Attila Mándi and Tibor Kurtán, Department of Organic Chemistry, University of Debrecen, PO Box 400, H-4002 Debrecen, Hungary.
Email: mandi.attila@science.unideb.hu; kurtan.tibor@science.unideb.hu

Funding information
National Research, Development and Innovation Office, Grant/Award Numbers: NKFI K120181, K112951 and PD121020; TÁMOP 4.2.4. A/2-11-1-2012-0001; Governmental Information-Technology Development Agency (KIFÜ)

Abstract

Synthesis of racemic hexahydropyrrolo[1,2-a]quinoline derivatives (**1**-**8**) was performed by utilizing the Knoevenagel-[1,5]-hydride shift-cyclization domino reaction. Separation of the enantiomers of the chiral products (**1**-**8**) was carried out by chiral high-performance liquid chromatography, and online high-performance liquid chromatography-electronic circular dichroism (ECD) spectra were recorded to elucidate the absolute configuration by comparing the experimental and time-dependent density functional theory-ECD spectra obtained at various theoretical levels. For 1 of the products, the time-dependent density functional theory-ECD calculations allowed determining both the relative and the absolute configuration by distinguishing the 4 stereoisomers. One of the compounds with spiro 1,3-cyclohexanedione moiety (**7**) possessed moderate acetylcholinesterase inhibitory activity, while **3** showed neuroprotective activity in oxygen-glucose deprivation-induced neurotoxicity in human neuroblastoma SH-SY5Y cells.

KEYWORDS

[1,5]-hydride shift, C-H activation, density functional theory, relative and absolute configuration

1 | INTRODUCTION

The substituted chiral 1,2,3,4-tetrahydroquinoline moiety is a common structural feature of alkaloid and antibiotic natural products possessing a wide range of biological activity such as anti-HIV, antimicrobial, anticonvulsant, antimalarial, and cytotoxic activities.[1] Moreover, substituted 1,2,3,4-tetrahydroquinoline derivatives can serve as building blocks for pharmaceuticals,[2] as well as for the total synthesis of some natural products.[3-5]

The Knoevenagel-[1,5]-hydride shift-cyclization cascade reaction of 2-trialkylamino-benzaldehydes, called also tertiary amino effect induced cyclization, provides a straightforward access to chiral 1,2,3,4-tetrahydroquinolines by the formation of the C-2—C-3 bond of the tetrahydroquinoline unit.[4] Starting from 2-(pyrrolidin-1-yl)benzaldehyde, a Knoevenagel-[1,5]-hydride shift-cyclization cascade reaction with reagents containing active methylene group had provided hexahydropyrrolo[1,2-a]quinoline derivatives,[6-8] the

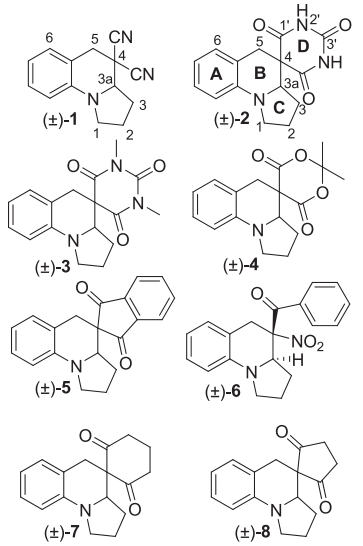

FIGURE 1 Structures of the studied hexahydropyrrolo[1,2-a] quinoline derivatives **1** to **8**

synthesis of which was also accomplished by intramolecular Schmidt reaction[9] and cyclization of in situ generated dialkoxytitanacyclopropane derivatives (Figure 1).[10] The absolute configurations of the enantiomers of chiral hexahydropyrrolo[1,2-a]quinoline derivatives have not been studied yet.

Herein, the synthesis of 5 known (**1**-**4** and **7**) and 3 new (**5**, **6**, and **8**) racemic hexahydropyrrolo[1,2-a]quinoline derivatives is presented. In addition, chiral high-performance liquid chromatography (HPLC) separation of their enantiomers and HPLC-electronic circular dichroism (ECD) analysis aided by time-dependent density functional theory ECD (TDDFT-ECD) calculations were achieved. The recent ECD calculations also provide an example for distinguishing 4 stereoisomers of **6** by the comparison of the computed ECDs of diastereomers with experimental data. Moreover, the acetylcholinesterase (AChE) inhibitory and neuroprotective activity of the products have been tested.

2 | MATERIALS AND METHODS

2.1 | General

High-performance liquid chromatography-ECD spectra were recorded on a J-810 spectropolarimeter. Chiral HPLC separations were carried out with a Jasco (Tokyo, Japan) HPLC system on Chiralpak columns by using different eluents.

2.2 | Computational section

Mixed torsional/low-frequency mode conformational searches were carried out by means of the Macromodel 9.9.223 software by using the Merck Molecular Force Field (MMFF) with an implicit solvent model for $CHCl_3$.[11] Geometry reoptimizations were carried out at the B3LYP/6-31G(d) level in vacuo, the B3LYP/TZVP, the B97D/TZVP,[12,13] and the CAM-B3LYP/TZVP[14,15] levels with the PCM solvent model for $CHCl_3$. Time-dependent density functional theory-ECD calculations were run with various functionals (B3LYP, BH&HLYP, CAM-B3LYP, and PBE0) and the TZVP basis set as implemented in the Gaussian 09 package with the same or no solvent model as in the preceding DFT optimization step.[16] Electronic circular dichroism spectra were generated as sums of Gaussians with 1800 to 3300 cm^{-1} widths at half-height (corresponding to ca. 12 to 22 nm at 260 nm), using dipole-velocity-computed rotational strength values.[17] Boltzmann distributions were estimated from the ZPVE-corrected B3LYP/6-31G(d) energies in the gas-phase calculations and from the B3LYP, B97D, and CAM-B3LYP energies in the solvated ones. The MOLEKEL software package was used for visualization of the results.[18]

3 | RESULTS AND DISCUSSION

2-(Pyrrolidin-1-yl)benzaldehyde (**11**) prepared from 2-fluorbenzaldehyde (**9**) and pirrolidine (**10**) as described in the literature[19] could be used as a suitable starting material for the 1-pot synthesis of hexahydropyrrolo[1,2-a]quinoline derivatives **1** to **8**. 2-(Pyrrolidin-1-yl)benzaldehyde (**11**) was reacted with cyclic 1,3-dicarbonyl derivatives or reagents containing active methylene group.

The domino reaction started with a Knoevenagel condensation (**11** → **12**) followed by an [1,5]-hydride shift

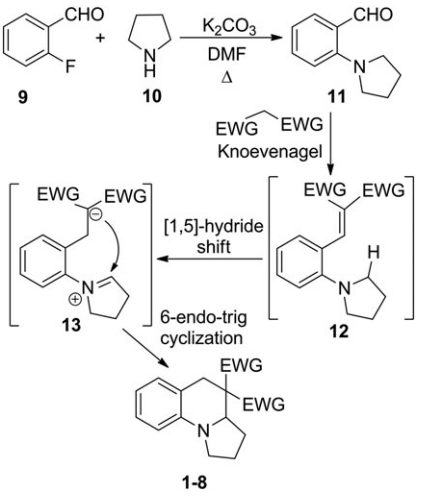

SCHEME 1 Preparation of the hexahydropyrrolo[1,2-a]quinoline derivatives **1** to **8** with the general mechanism of the domino reaction

(**12** → **13**) and a 6-endo-trig cyclization (**13** → **1**-**8**) as shown in Scheme 1. In the case of the dicyano derivative **1**, the corresponding Knoevenagel product **12** could be also isolated confirming the mechanism.

Although stereoselective [1,5]-hydride shift-cyclization cascade reaction of 1,3-diester Knoevenagel intermediates using enantioselective catalysis with chiral metal complexes[20,21] or organocatalysts[22,23] was reported, similar enatioselective reactions are not available for the reagent applied for the synthesis of **1** to **8**. Enantiomers of the prepared racemic **1** to **8** were separated by Chiralpak IA, IC, or IB columns by using hexane/2-propanol, hexane/dichloromethane, *tert*-butyl-methyl ether/propan-2-ol, or *tert*-butyl-methyl ether/ethanol eluent combinations. Due to the different chromophores at the tetrasubstituted C-4 carbon, the HPLC-ECD spectra of the separated enantiomers of **1** to **8** were quite different requiring TDDFT-ECD analysis for most of them to determine the absolute configuration. The combination of HPLC-ECD measurements and TDDFT-ECD calculations was proved an efficient tool to study the absolute configuration of stereoisomers derived from racemic or scalemic mixtures of synthetic and natural origin.[24-26]

For the configurational assignment, preliminary MMFF conformers were generated in a conformational search, these conformers were reoptimized at several DFT levels [B3LYP/6-31G(d) in vacuo, B3LYP/TZVP, B97D/TZVP, and CAM-B3LYP with PCM for $CHCl_3$], and ECD spectra were computed with various functionals (B3LYP, BH&HLYP, CAM-B3LYP, and PBE0) and the TZVP basis set with or without the same solvent model as applied in the preceding DFT optimization step.

Enantiomers of the dicyano derivative **1** were baseline separated on a Chiralpak IC column with eluent system hexane/2-propanol 70:30, and mirror image HPLC-ECD spectra were recorded. The MMFF conformational search of the arbitrarily chosen (*R*)-**1** resulted in 3 conformers, the B3LYP/6-31G(d) reoptimization of which yielded 2 conformers over 1% Boltzmann-population. These conformers differed slightly in the puckering of ring C and the orientation of the cyano groups (Figure 2).

The 2 conformers exhibited rather similar computed ECD spectra, and their Boltzmann-weighted ECD

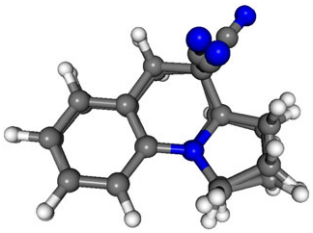

FIGURE 2 Overlapped structures of the 2 low-energy B3LYP/6-31G(d) conformers of (*R*)-**1**

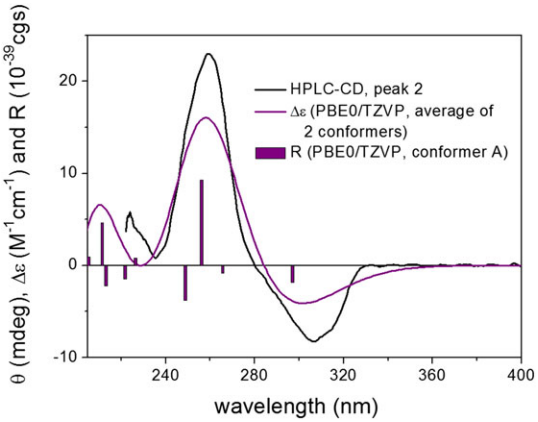

FIGURE 3 High-performance liquid chromatography-electronic circular dichroism (ECD) spectrum of the second-eluting enantiomer of **1** (black line) compared with the time-dependent density functional theory (DFT)-ECD spectrum of (*R*)-**1** (purple line: Boltzmann-weighted PBE0/TZVP ECD spectrum of the 2 low-energy solution conformers. Level of DFT optimization: B3LYP/6-31G[d]). The bars represent rotational strength values for the lowest-energy solution conformer

spectrum reproduced well the experimental HPLC-ECD spectrum of the second-eluting enantiomer allowing the unambiguous determination of the absolute configuration; the first-eluting enantiomer has (*S*) and the second-eluting one (*R*) absolute configuration (Figure 3).

Enantiomers of **3** obtained in the reaction with *N*,*N*-dimethylbarbituric acid were separated on Chiralpak IA column by using hexane/2-propanol 80:20 eluent. The HPLC-ECD spectra of the separated enantiomers of **3** were completely different from those of **1**, and hence, ECD calculations were required for the configurational assignment. The MMFF conformational search of the arbitrarily chosen (*S*) enantiomer of **3** resulted in 4 conformers, the DFT level reoptimizations of which yielded 2 to 3 conformers over 1% Boltzmann-population

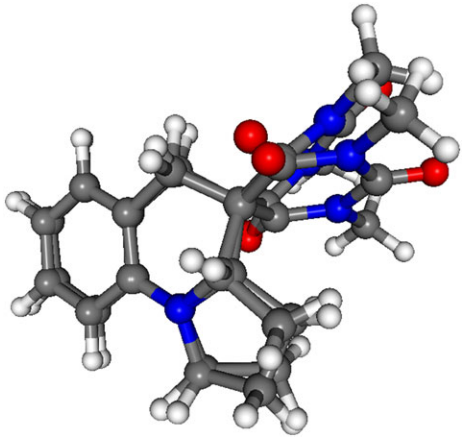

FIGURE 4 Overlapped structures of the 2 low-energy conformers of (*S*)-**3** obtained at the CAM-B3LYP/TZVP PCM/$CHCl_3$ level of theory

depending on the applied level (Figure 4). Similarly to **1**, these conformers differed in the puckering of ring C and D, but conformational differences were larger than for **1**, especially with the B97D functional (results not shown).

Electronic circular dichroism spectra computed for the individual conformers obtained at various DFT levels gave moderate to good agreement with the experimental HPLC-ECD spectrum of the second-eluting enantiomer allowing elucidation of the absolute configuration as (*S*) for the second-eluting enantiomer and (*R*) for the first-eluting one. The best agreement was achieved by the CAM-B3LYP/TZVP PCM/$CHCl_3$ ECD spectrum of the CAM-B3LYP/TZVP PCM/$CHCl_3$ conformers (Figure 5).

Simple comparison of HPLC-ECD spectrum of **3** with that of **2** has clearly shown that the absence of *N*-methyl groups did not change the HPLC-ECD spectra significantly. The HPLC-ECD spectrum of the first-eluting enantiomers showed in both cases −/+/+/−/+ ECD pattern from the low-energy to the high-energy region allowing assignment of (*R*) absolute configuration (see Supplementary Data).

Meldrum's acid was used as a reagent for the preparation of **4**, the enantiomers of which were baseline separated on a Chiralpak IA column with hexane/2-propanol 90:10 eluent. Due to the same position of the ester and amide carbonyl groups, the separated enantiomers of **4** showed quite similar HPLC-ECD spectra to those of **3**. The MMFF conformational search of the arbitrarily chosen (*S*) enantiomer resulted in 8 conformers, the DFT level reoptimizations of which yielded 3 conformers over 1% Boltzmann-population at all the applied levels of theory. Conformers had minor variations in the conformation of the lactone and pyrrolidine rings (Figure 6).

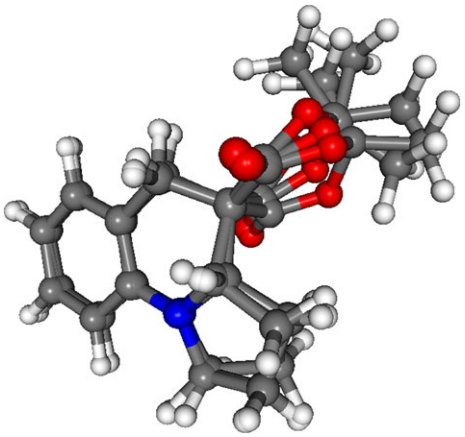

FIGURE 6 Overlapped structures of the 3 low-energy conformers of (*S*)-**4** obtained at the CAM-B3LYP/TZVP PCM/$CHCl_3$ level of theory

Boltzmann averaged ECD spectra of the low-energy conformers resembled the experimental HPLC-ECD spectrum of the second-eluting enantiomer allowing elucidation of the absolute configuration as (*S*) for the second-eluting enantiomer and (*R*) for the first one. It is interesting to note that ECD spectra computed with the BH&HLYP and CAM-B3LYP functionals gave good agreement for all conformers obtained from various DFT reoptimizations, while the PBE0 and especially the B3LYP functionals gave moderate to poor agreement with the experimental spectrum (Figure 7). These results are in line with the findings of Pescitelli and Bruhn,[27] which

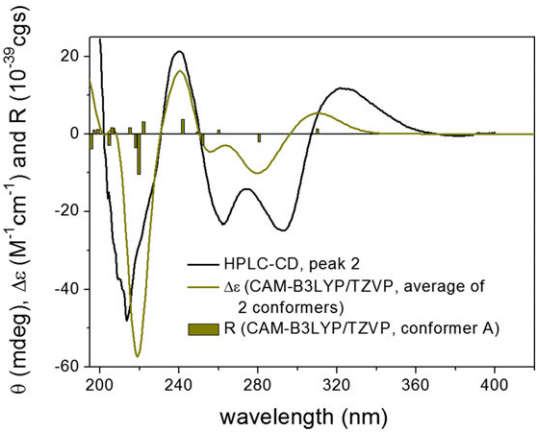

FIGURE 5 High-performance liquid chromatography-electronic circular dichroism (ECD) spectrum of the second-eluting enantiomer of **3** (black line) compared with the time-dependent density functional theory (DFT)-ECD spectrum of (*S*)-**3** (olive line: Boltzmann-weighted CAM-B3LYP/TZVP PCM/$CHCl_3$ ECD spectrum of the 2 low-energy solution conformers. Level of DFT optimization: CAM-B3LYP/TZVP PCM/$CHCl_3$). The bars represent rotational strength values for the lowest-energy solution conformer

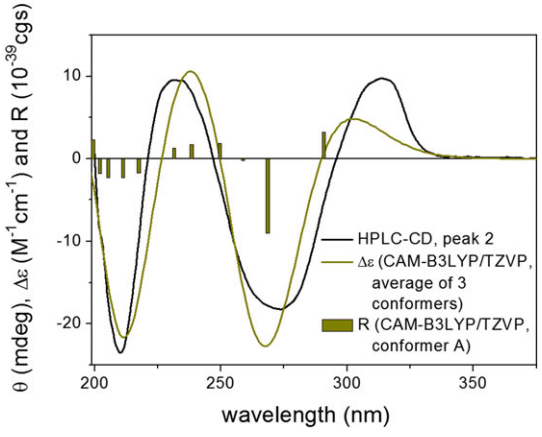

FIGURE 7 High-performance liquid chromatography-electronic circular dichroism (ECD) spectrum of the second-eluting enantiomer of **4** (black line) compared with the time-dependent density functional theory (DFT)-ECD spectrum of (*S*)-**4** (dark yellow line: Boltzmann-weighted CAM-B3LYP/TZVP PCM/$CHCl_3$ ECD spectrum of the 2 low-energy solution conformers. Level of DFT optimization: CAM-B3LYP/TZVP PCM/$CHCl_3$). The bars represent rotational strength values for the lowest-energy solution conformer

recommended using simultaneously more than 1 level of theory for both DFT optimization and ECD calculation and stated that there is no superior method, which could be applied with confidence for every case.

Compound **5** was prepared in the reaction with indan-1,3-dione, and enantiomers were baseline separated on a Chiralpak IC column by using hexane/dichloromethane 70:30 eluent. Due to the different chromophore, the HPLC-ECD spectra of the separated enantiomers were markedly different from those of all the other derivatives. The MMFF conformational search of (*R*)-**5** resulted in 3 conformers, the DFT reoptimizations of which yielded 2 conformers over 1% Boltzmann-population at all the applied levels of theory (Figures 8 and 9). The 2 conformers differed in the orientation of the C-2 pyrrolidine methylene group, and they had different computed ECD spectra. Both the gas phase BH&HLYP/TZVP//B3LYP/6-31G(d) (Figure 10) and the PCM solvent model BH&HLYP/TZVP PCM/$CHCl_3$//B3LYP/TZVP PCM/$CHCl_3$ (Figure 11) calculations gave sufficiently good agreement for the unambiguous determination of absolute configuration.

Interestingly, the gas-phase calculations reproduced well the 236-nm positive shoulder but failed to give the 297-nm positive Cotton effect, while the same B3LYP functional with PCM solvent model for the conformers optimized at higher level and with PCM model reproduced the 297-nm Cotton effect satisfactorily and failed for the 236-nm shoulder. The B97D and CAM-B3LYP functionals were also tested for the DFT reoptimization but could not significantly improve the solvent model B3LYP results.

Compound **6** was obtained with the unsymmetrical reagent 2-nitro-1-phenylethanone, and thus, in contrast to the previous examples, the tetrasubstituted C-4 carbon

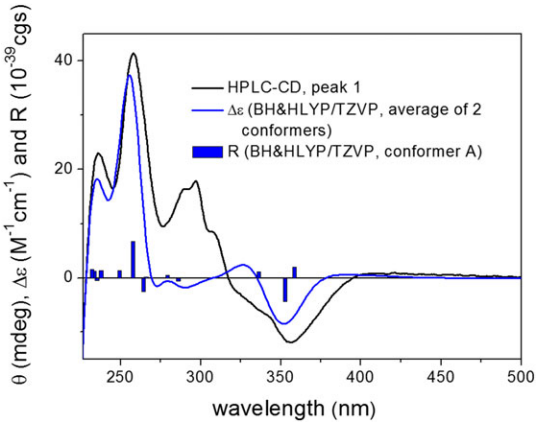

FIGURE 10 High-performance liquid chromatography-electronic circular dichroism (ECD) spectrum of the first eluting enantiomer of **5** (black line) compared with the time-dependent density functional theory (DFT)-ECD spectrum of (*R*)-**5**, (blue line: Boltzmann-weighted BH&HLYP/TZVP ECD spectrum of the 2 low-energy solution conformers. Level of DFT optimization: B3LYP/6-31G[d]). The bars represent rotational strength values for the lowest-energy solution conformer

became a chirality center. The determination of the relative configuration for 2 newly established chirality centers could not be unambiguously carried out by NOE measurements because of the tetrasubstituted C-4 chirality center. The enantiomers of **6** were separated on a Chiralpak IA column using hexane/2-propanol 95:5 eluent, and HPLC-ECD spectra aided with conformational analysis and ECD calculations were used to distinguish the 4 possible stereoisomers. The MMFF conformational search of the (3a*R*,4*R*) and (3a*R*,4*S*) diastereomers resulted in 10 and 4 conformers, respectively, reoptimization of which at both the B3LYP/6-31G(d) and the B3LYP/TZVP PCM/$CHCl_3$ levels yielded 2 low-

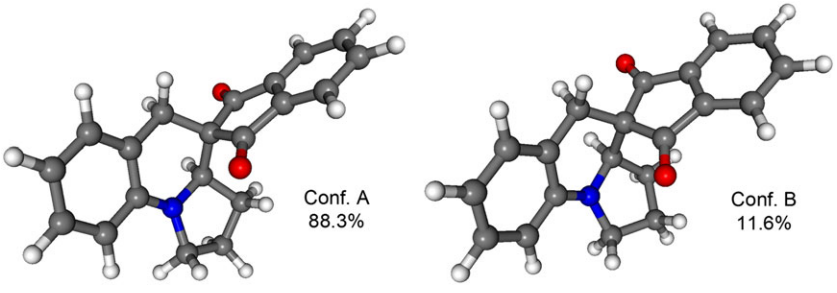

FIGURE 8 Low-energy conformers (≥1%) of (*R*)-**5** obtained at B3LYP/6-31G(d) level of theory

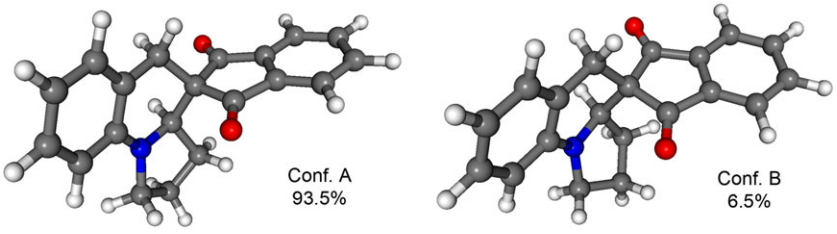

FIGURE 9 Low-energy conformers (≥1%) of (*R*)-**5** obtained at B3LYP/TZVP PCM/$CHCl_3$ level of theory

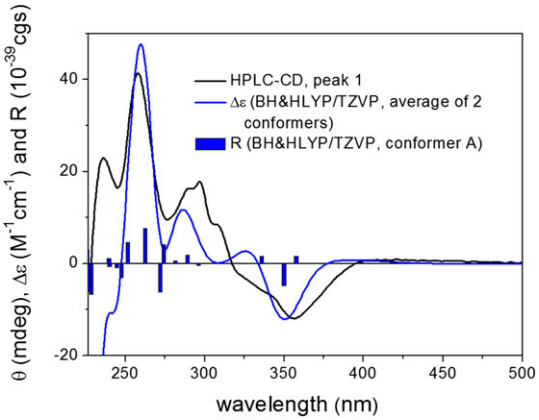

FIGURE 11 High-performance liquid chromatography-electronic circular dichroism (ECD) spectrum of the first-eluting enantiomer of **5** (black line) compared with the time-dependent density functional theory (DFT)-ECD spectrum of (*R*)-**5** (blue line: Boltzmann-weighted BH&HLYP/TZVP PCM/$CHCl_3$ ECD spectrum of the 2 low-energy solution conformers. Level of DFT optimization: B3LYP/TZVP PCM/$CHCl_3$). The bars represent rotational strength values for the lowest-energy solution conformer

energy conformers over 1% Boltzmann population for both diastereomers (Figures 12 and 13).

Electronic circular dichroism spectra computed for both sets of conformers allowed distinguishing the 4 stereoisomers because the (3a*R*,4*R*) diastereomer showed good agreement with the first-eluting enantiomer (Figure 14), while the (3a*R*,4*S*) diastereomer had a completely different ECD pattern (Figure 15). Consequently, the first-eluting enantiomer has (3a*R*,4*R*) and the second one (3a*S*,4*S*) absolute configuration. This ECD calculation represents a further example, in which not only enantiomers but also diastereomers could be distinguished by TDDFT-ECD calculations supporting the determination of the relative configuration.[28-30]

Compound **7** was prepared in the reaction with cyclohexane-1,3-dione, and enantiomers were separated on Chiralpak IB column by using *tert*-butyl-methyl ether/propan-2-ol 98:2 as eluent. The MMFF conformational search of the arbitrarily chosen (*S*) enantiomer resulted

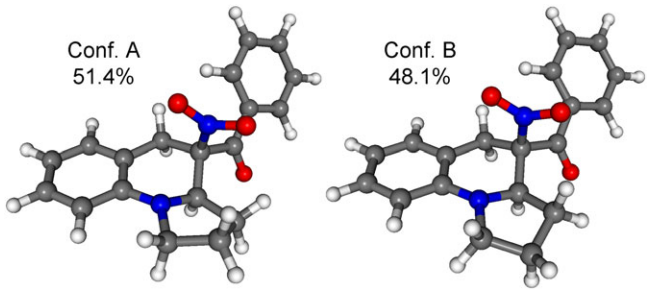

FIGURE 12 Low-energy conformers (≥1%) of (3a*R*,4*R*)-**6** obtained at the B3LYP/TZVP PCM/$CHCl_3$ level of theory

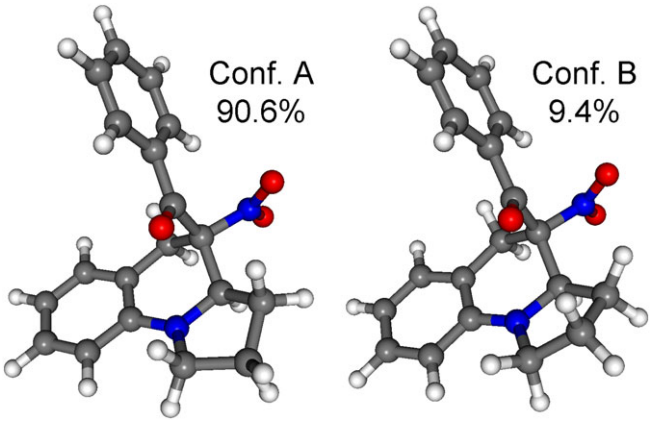

FIGURE 13 Low-energy conformers (≥1%) of (3a*R*,4*S*)-**6** obtained at the B3LYP/TZVP PCM/$CHCl_3$ level of theory

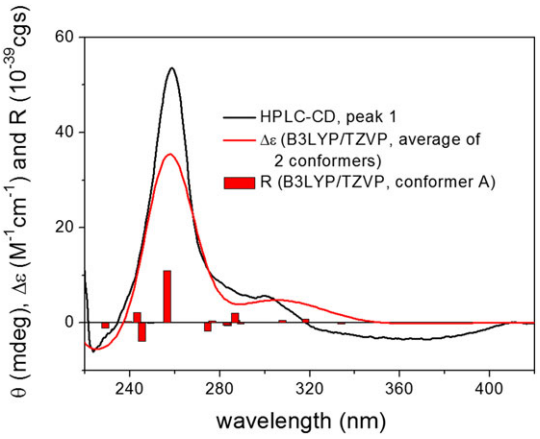

FIGURE 14 High-performance liquid chromatography-electronic circular dichroism (ECD) spectrum of the first-eluting enantiomer of **6** (black line) compared with the time-dependent density functional theory (DFT)-ECD spectrum of (3a*R*,4*R*)-**6** (red line: Boltzmann-weighted B3LYP/TZVP PCM/$CHCl_3$ ECD spectrum of the 2 low-energy solution conformers. Level of DFT optimization: B3LYP/TZVP PCM/$CHCl_3$). The bars represent rotational strength values for the lowest-energy solution conformer

in 7 conformers, the DFT reoptimizations of which yielded 3 to 4 conformers over 1% Boltzmann-population at all the applied levels of theory (Figure S41). Despite the similarity of geometries of the computed conformers (differing only in the puckering of rings C and D) as well as the computed ECD spectra of the individual conformers, the experimental HPLC-ECD spectra could not be reproduced satisfactorily (Figure S42). Furthermore, the B3LYP and PBE0 functionals gave significantly different results from those of the BH&HLYP and CAM-B3LYP. The HPLC-UV chromatograms of **7** and **8** suggested that partial enolization is feasible because an elevated baseline connected the separated enantiomers of **8** (Figures S39 and S48). This was further confirmed by the ^{13}C-NMR

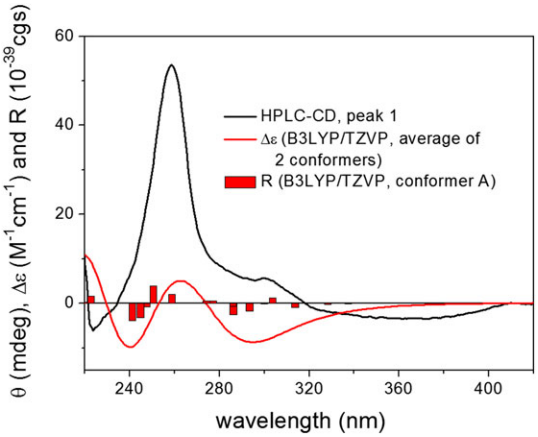

FIGURE 15 High-performance liquid chromatography-electronic circular dichroism (ECD) spectrum of the first-eluting enantiomer of **6** (black line) compared with the time-dependent density functional theory (DFT)-ECD spectrum of (3a*R*,4*S*)-**6** (red line: Boltzmann-weighted B3LYP/TZVP PCM/$CHCl_3$ ECD spectrum of the 2 low-energy solution conformers. Level of DFT optimization: B3LYP/TZVP PCM/$CHCl_3$). The bars represent rotational strength values for the lowest-energy solution conformer

spectrum, which showed an additional set of signals with small intensity belonging to the enol tautomer(s). Therefore, the above calculations were also performed on the possible enol forms, but even using various ratios of the parent compound **7** and its possible enol tautomers could not improve the ECD agreement. It is worth mentioning that in the enol tautomer, the spiro carbon atom becomes a chirality center, which can contribute to the bad agreement of the computed ECD spectra.

By considering only the first 2 transitions of the B3LYP and PBE0 ECD spectra or the first 3 of the BH&HLYP and CAM-B3LYP ones of the parent compound **7**, (*S*) absolute configuration could be tentatively assigned for the first-eluting enantiomer and (*R*) for the second one. The (*S*) absolute configuration of the first-eluting enantiomer is also in line with the results of the closely related **8**, for which the first 3 major ECD transitions had the same sign for the first-eluting (*S*) enantiomer separated under similar conditions (vide infra).

Compound **8** was obtained in the domino reaction with cyclopentane-1,3-dione, and enantiomers were separated on Chiralpak IB column by using *tert*-butyl-methyl ether/ethanol 95:5 eluent. The MMFF conformational search of the arbitrarily chosen (*R*) enantiomer resulted in 4 conformers, the DFT level reoptimizations of which yielded 2 conformers over 1% Boltzmann-population at all the applied levels of theory. Similarly to **7**, the conformers differed only in the puckering of rings C and D (Figure 16).

Overall ECD spectra obtained at almost each combination of theoretical levels applied for the DFT and the ECD computational steps gave consistent moderate to good

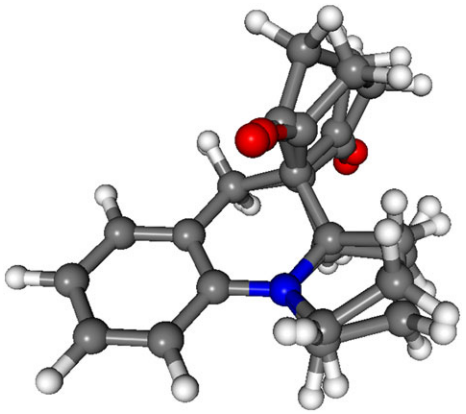

FIGURE 16 Overlapped structures of the 2 low-energy conformers of (*R*)-**8** obtained at the CAM-B3LYP/TZVP PCM/$CHCl_3$ level of theory

agreement with the second-eluting enantiomer allowing elucidation of the absolute configuration as (*R*) for this enantiomer and (*S*) for the first-eluting one (Figure 17). It is interesting to note that the B3LYP and PBE0 functionals reproduced better the low-energy region while the BH&HLYP and CAM-B3LYP functionals performed better for the 260-nm transition (Figure 17). Best agreements were achieved for the CAM-B3LYP PCM and the B3LYP in vacuo conformers, while the B97D PCM calculations gave the worst agreement with the BH&HLYP and CAM-B3LYP functionals which were found the best for **4**. This result further supports the importance of the parallel application of various DFT functionals for both the geometry optimization and the ECD calculation steps.[13,27,31]

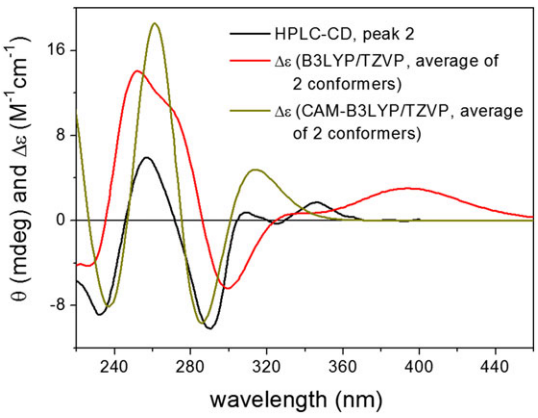

FIGURE 17 High-performance liquid chromatography-electronic circular dichroism (ECD) spectrum of the second-eluting enantiomer of **8** (black line) compared with the time-dependent density functional theory (DFT)-ECD spectra of (*R*)-**8** (red line: Boltzmann-weighted B3LYP/TZVP PCM/$CHCl_3$ ECD spectrum of the 2 low-energy solution conformers; dark yellow line: Boltzmann-weighted CAM-B3LYP/TZVP PCM/$CHCl_3$ ECD spectrum of the 2 low-energy solution conformers. Level of DFT optimization: CAM-B3LYP/TZVP PCM/$CHCl_3$)

Acetylcholinesterase inhibitory activity of the products was tested, and *rac*-**7** was found to show moderate AChE inhibitory activity with 35.4% inhibition at 40-μM concentration. The neuroprotective activities of the products were also tested against hydrogen peroxide (H_2O_2), β-amyloid-25-35 fragment ($A\beta_{25\text{-}35}$), and oxygen-glucose deprivation-induced neurotoxicity in human neuroblastoma SH-SY5Y cells. The preliminary screenings showed that *rac*-**3** at 1-μM concentration displayed neuroprotective activity against oxygen-glucose deprivation-induced cellular injuries in human neuroblastoma SH-SY5Y cells with 18.6% increase in cell viability.

4 | CONCLUSION

Eight chiral hexahydropyrrolo[1,2-a]quinoline derivatives were prepared in a Knoevenagel-[1,5]-hydride shift-cyclization cascade reaction. The enantiomers of **1** to **8** could be separated by chiral HPLC whose absolute configuration was determined by means of HPLC-ECD and TDDFT-ECD calculations. The correlation of the absolute configuration with ECD data for hexahydropyrrolo[1,2-a] quinoline derivatives may help the future enantioselective version of the domino reaction. For the product obtained with 2-nitro-1-phenylethanone, not only enantiomers but also diastereomers could be distinguished by ECD calculations aiding the assignment of the relative configuration.

ACKNOWLEDGMENTS

The authors thank the National Research, Development and Innovation Office (grant nos. NKFI K120181, K112951, and PD121020) for financial support and the CPU time by the Governmental Information-Technology Development Agency (KIFÜ). The computational stereochemical studies of **5** were realized in the frames of TÁMOP 4.2.4. A/2-11-1-2012-0001 National Excellence Program—Elaborating and operating an inland student and researcher personal support system convergence program.

ORCID

Attila Mándi http://orcid.org/0000-0002-7867-7084
Tibor Kurtán http://orcid.org/0000-0002-8831-8499

REFERENCES

1. Sridharan V, Suryavanshi PA, Menendez JC. Advances in the chemistry of tetrahydroquinolines. *Chem Rev*. 2011;111(11):7157-7259.
2. Gosmini R, Nguyen VL, Toum J, et al. The discovery of I-BET726 (GSK1324726A), a potent tetrahydroquinoline ApoA1 up-regulator and selective BET bromodomain inhibitor. *J Med Chem*. 2014;57(19):8111-8131.
3. Wang T, Zhuo L-G, Li Z, et al. Highly enantioselective hydrogenation of quinolines using phosphine-free chiral cationic ruthenium catalysts: scope, mechanism, and origin of enantioselectivity. *J Am Chem Soc*. 2011;133(25):9878-9891.
4. Meth-Cohn O. The t-amino effect: heterocycles formed by ring closure of ortho-substituted t-anilines. In: Katriczky AR, ed. *Advances in heterocyclic chemistry*. San Diego: Academic Press, Inc; 1996:1-37.
5. Mátyus P, Eliás O, Tapolcsányi P, Polonka-Bálint A, Halász-Dajka B. Ring-closure reactions of ortho-vinyl-tert-anilines and (di)aza-heterocyclic analogues via the tert-amino effect: recent developments. *Synthesis*. 2006;2006(16):2625-2639.
6. Groenen LC, Verboom W, Nijhuis WHN, Reinhoudt DN, Van Hummel GJ, Feil D. The tertiary amino effect in heterocyclic synthesis: mechanistic and computational study of the formation of six-membered rings. *Tetrahedron*. 1988;44(14):4637-4644.
7. Rabong C, Hametner C, Mereiter K, Kartsev VG, Jordis U. Scope and limitations of the T-reaction employing some functionalized C-H-acids and naturally occurring secondary amines. *Heterocycles*. 2008;75(4):799-838.
8. Platonova AY, Poluikova AA, Glukhareva TV, Morzherin YY. Synthesis of fused 3-cyano- and 3-carbamoyl-1,2,3,4-tetrahydroquinolines. *Russ Chem Bull*. 2014;63(7):1580-1583.
9. Pearson WH, Fang W. Synthesis of benzo-fused 1-azabicyclo[m.n.0]alkanes via the Schmidt reaction: a formal synthesis of gephyrotoxin. *J Org Chem*. 2000;65(21):7158-7174.
10. Lee J, Ha JD, Cha JK. New synthetic method for functionalized pyrrolizidine, indolizidine, and mitomycin alkaloids. *J Am Chem Soc*. 1997;119(34):8127-8128.
11. MacroModel. Schrödinger LLC, 2012. http://www.schrodinger.com/MacroModel.
12. Grimme S. Semiempirical GGA-type density functional constructed with a longrange dispersion correction. *J Comput Chem*. 2006;27(15):1787-1799.
13. Sun P, Xu DX, Mándi A, et al. Structure, absolute configuration, and conformational study of 12-membered macrolides from the fungus Dendrodochium sp. associated with the sea cucumber Holothuria nobilis Selenka. *J Org Chem*. 2013;78(14):7030-7047.
14. Yanai T, Tew D, Handy N. A new hybrid exchange-correlation functional using the Coulomb-attenuating method (CAM-B3LYP). *Chem Phys Lett*. 2004;393(1-3):51-57.
15. Pescitelli G, Bari DL, Berova N. Conformational aspects in the studies of organic compounds by electronic circular dichroism. *Chem Soc Rev*. 2011;40(9):4603-4625.
16. Frisch MJ, Trucks GW, Schlegel HB, et al. *Gaussian 09, Revision B.01*. Wallingford CT, Gaussian; 2010.
17. Stephens PJ, Harada N. ECD cotton effect approximated by the Gaussian curve and other methods. *Chirality*. 2010;22(2):229-233.
18. Varetto U. MOLEKEL, v. 5.4, Swiss National Supercomputing Centre, Manno, Switzerland, 2009.

19. Han YY, Han WY, Hou X, Zhang XM, Yuan WC. $FeCl_3$-catalyzed stereoselective construction of spirooxindole tetrahydroquinolines via tandem 1,5-hydride transfer/ring closure. *Org Lett*. 2012;14(16):4054-4057.
20. Cao W, Liu X, Wang W, Lin L, Feng X. Highly enantioselective synthesis of tetrahydroquinolines via cobalt(II)-catalyzed tandem 1,5-hydride transfer/cyclization. *Org Lett*. 2011;13(4):600-603.
21. Murarka S, Deb I, Zhang C, Seidel D. Catalytic enantioselective intramolecular redox reactions: ring-fused tetrahydroquinolines. *J Am Chem Soc*. 2009;131(37):13226-13227.
22. Chen L, Zhang L, Lv J, Cheng JP, Luo S. Catalytic enantioselective tert-aminocyclization by asymmetric binary acid catalysis (ABC): stereospecific 1,5-hydrogen transfer. *Chem A Eur J*. 2012;18(29):8891-8895.
23. Mori K, Ehara K, Kurihara K, Akiyama T. Selective activation of enantiotopic C(sp^3) hydrogen by means of chiral phosphoric acid: asymmetric synthesis of tetrahydroquinoline derivatives. *J Am Chem Soc*. 2011;133(16):6166-6169.
24. Tóth L, Fu Y, Zhang HY, et al. Preparation of neuroprotective condensed 1,4-benzoxazepines by regio- and diastereoselective domino Knoevenagel-[1,5]-hydride shift-cyclization reaction. *Beilstein J Org Chem*. 2014;10:2594-2602.
25. Meng LH, Mándi A, Li XM, Liu Y, Kurtán T, Wang BG. Isolation, stereochemical study, and antioxidant activity of benzofuranone derivatives from a mangrove-derived fungus Eurotium rubrum MA-150. *Chirality*. 2016;28(8):581-584.
26. Tóth B, Liktor-Busa E, Kusz N, et al. Phenanthrenes from Juncus inflexus with antimicrobial activity against methicillin-resistant Staphylococcus aureus. *J Nat Prod*. 2016;79(11):2814-2823.
27. Pescitelli G, Bruhn T. Good computational practice in the assignment of absolute configurations by TDDFT calculations of ECD spectra. *Chirality*. 2016;28(6):466-474.
28. Liang LF, Kurtán T, Mándi A, et al. Sarsolenane and capnosane diterpenes from the Hainan soft coral Sarcophyton trocheliophorum Marenzeller as PTP1B inhibitors. *Eur J Org Chem*. 2014;2014(9):1841-1847.
29. Zhang P, Meng LH, Mándi A, et al. 4-oxoquinoline and indole alkaloids with C-2 reversed prenylation from the mangrove-derived endophytic fungus Penicillium brocae. *Eur J Org Chem*. 2014;2014(19):4029-4036.
30. Ancheeva E, Küppers L, Akone SH, et al. Expanding the metabolic profile of the fungus Chaetomium sp. through co-culture with autoclaved Pseudomonas aeruginosa. *Eur J Org Chem*. 2017;2017(22):3256-3264.
31. Ilkei V, Spaits A, Prechl A, et al. Biomimetic synthesis and HPLC-ECD analysis of the isomers of dracocephins A and B. *Beilstein J Org Chem*. 2016;12:2523-2534.

SUPPORTING INFORMATION

Additional supporting information may be found online in the Supporting Information section at the end of the article.

How to cite this article: Tóth L, Mándi A, Váradi D, et al. HPLC-ECD and TDDFT-ECD study of hexahydropyrrolo[1,2-a]quinoline derivatives. *Chirality*. 2018;1–9. https://doi.org/10.1002/chir.22969